Graphene Quantum Dots as Universal Fluorophores and Their Use in Revealing Regulated Trafficking of Insulin Receptors in Adipocytes

Xin Ting Zheng, Aung Than, Arundithi Ananthanaraya, Dong-Hwan Kim, and Peng Chen*

Division of Bioengineering, School of Chemical & Biomedical Engineering, Nanyang Technological University, Singapore 637457

ABSTRACT Graphene quantum dots (GQDs) hold great promise as a new class of fluorophores for bioimaging, owing to their remarkable physicochemical properties including tunable photoluminescence, excellent photostability, and biocompatibility. Despite their highly anticipated potentials, GQDs have yet to be used to specifically label and track molecular targets involved in dynamic cellular processes in live cells. Here, we demonstrate that GQDs can serve as universal fluorophores for bioimaging because they can be readily conjugated with a wide range of biomolecules while preserving their functionalities. As a proof-of-concept demonstration, insulin-conjugated GQDs have been synthesized and utilized for specific labeling and dynamic tracking of insulin receptors in 3T3-L1 adipocytes. Our experiments reveal, for the first time, that the internalization and recycling of insulin receptors in adipocytes are oppositely regulated by apelin and TNFα, which may contribute to the regulations of these two cytokines in insulin sensitivity.

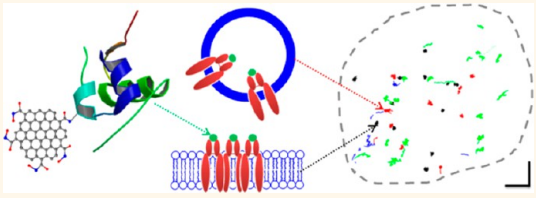

KEYWORDS: graphene quantum dot · fluorophore · insulin receptors · apelin · TNFα

Real-time tracking of fluorophore-tagged biomolecules is instrumental to reveal the dynamic cell functions at the single-cell or subcellular level.[1−3] An ideal fluorophore should be conveniently excitable, bright, stable, equipped with chemical handles for ready conjugation with target molecules, biocompatible, and small enough to minimize physical hindrance.[4] Currently, organic dyes and fluorescent proteins are predominantly used for bioimaging. They, however, intrinsically suffer from poor photostability, which makes long-term imaging challenging because of fast photobleaching. In addition, labeling with fluorescent proteins involves nontrivial molecular biology processes including construction of chimeric plasmids and subsequent transfection in live cells, and the abundance of expressed chimeric fluorescent proteins is often low due to ineffective hijacking of the native genetic machinery and the damages or cytotoxicity caused by the transfection procedure.

Semiconductor quantum dots (QDs) have been regarded as a promising alternative to organic fluorophores because of their high brightness and photostability.[1,4] They have been successfully employed for live-imaging of various cellular processes.[5−7] But QDs are toxic due to leaching of heavy metal ions, and since they are much larger (typically >500 kDa) than a biomolecule, they may alter the function and trafficking of the target molecule. For example, steric hindrance introduced by such a large tag may prevent the binding of the target molecule with its receptor. Also because of its large size, one QD carries multiple target molecules, creating an artificial cluster that may lead to unphysiological consequences. Their proneness to aggregation and their usual need for polymeric functional coating further exaggerate the aforementioned "size" issues.

Recently, graphene quantum dots (GQD, a single-atom-thick and nanometer-sized planar sheet of graphitic carbon) have sparked significant excitement as a promising new class of fluorophores for bioimaging, owing to their interesting and tunable photoluminescence properties originating from quantum confinement, excellent photostability, biocompatibility, good water solubility, chemical inertness, small size, and low

* Address correspondence to chenpeng@ntu.edu.sg.

Received for review May 7, 2013 and accepted June 25, 2013.

Published online June 25, 2013
10.1021/nn4023137

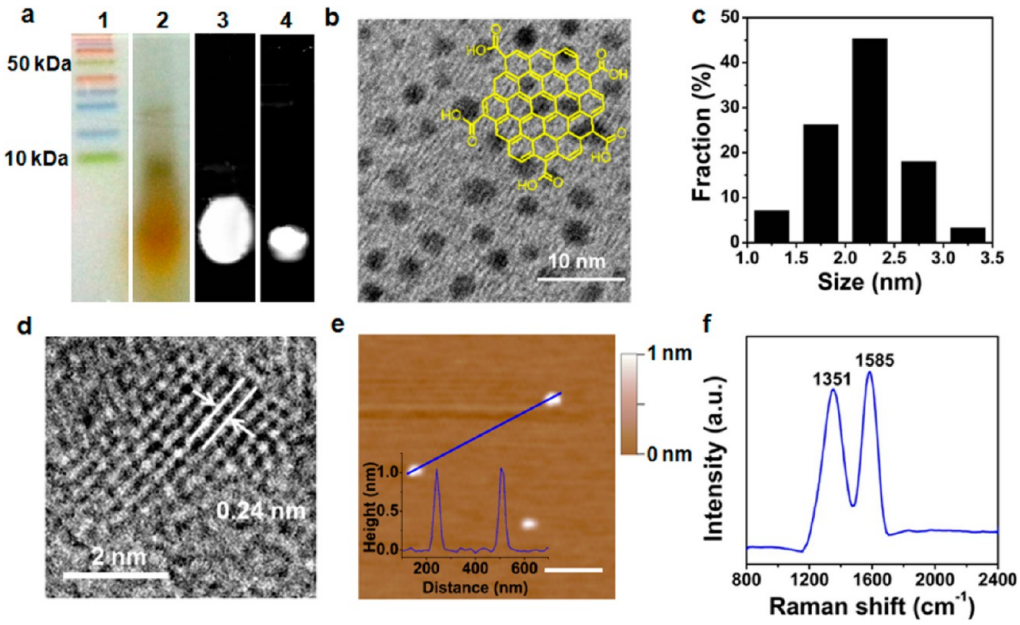

Figure 1. GQD characterizations. (a) Electrophoretic separation of molecular weight markers (1), GQDs (2 and 3), and GQDs after ultrafiltration (4). Lanes 1 and 2 were imaged under white light, while 3 and 4 were illuminated by a xenon lamp with a 488/505 nm filter. (b) TEM image of GQDs. Inset shows the chemical structure of a GQD. (c) Size distribution of 180 GQDs. (d) High-resolution TEM image. (e) AFM image of GQDs. Inset shows the height profile along the blue line. Scale bar = 0.2 μm. (f) Raman spectrum of GQDs.

cost.[8−20] Several groups have demonstrated that GQDs can be taken up into live cells and remain fluorescent in various cellular locations without introducing apparent cytotoxity, indicating the bioimaging capability of GQDs.[21−24] In a pioneer work, Dai and coworkers have shown that PEG-modified nanographene oxide sheets (~20 nm) functionalized with anti-CD20 can act as near-infrared fluorophores for selective recognition and imaging of CD20-expressing Raji B-cells.[25]

Despite their highly anticipated potentials, GQDs have yet to be used to specifically label and track molecular targets involved in dynamic cellular processes in live cells. Here, we demonstrate that GQDs can serve as universal fluorophores for bioimaging because they can be readily conjugated with a wide range of biomolecules without interfering with their activities. Moreover, we demonstrate the use of insulin-conjugated GQDs for real-time tracking of the dynamics of insulin receptors in 3T3-L1 adipocytes, using total internal reflection microscopy (TIRFM). Our experiments reveal, for the first time, that the internalization and recycling of insulin receptors in adipocytes were enhanced by apelin but inhibited by TNFα, providing evidence for the molecular mechanisms underlying the regulation of these cytokines in insulin sensitivity.

RESULTS AND DISCUSSION

GQDs were synthesized as previously reported,[26] but as shown in Figure 1a, the as-prepared GQDs separate into a fast-moving fluorescent band and a slow-moving nonfluorescent band by gel electrophoresis, indicating the existence of two heterogeneous populations differing in size. Therefore, ultrafiltration was used to eliminate larger nonfluorescent species. As shown in Figure 1a, the purified GQDs exhibit a narrow fluorescent band after electrophoresis, indicating the improved uniformity in size distribution. A comparison with the blots from known protein markers suggests that the electrophoretic mobility (thus probably the size) of the purified GQDs is comparable to a protein of a few kDa. The quantum yield of the purified GQDs is measured to be ~14.3%, which is much higher than that of the as-prepared GQDs (~4.04%).

As revealed by transmission electron microscopy (TEM), the obtained GQDs have an average diameter of ~2.2 nm with a narrow size distribution (Figure 1b and c). The molecular weight of such a GQD (2.2 nm atomic carbon sheet) is estimated to be ~2 kDa, consistent with the observation from gel electrophoresis. This molecular weight is desirably much smaller than a 6 nm CdSe quantum dot (~500 kDa) and the commonly used green fluorescent protein (27 kDa). It is also much smaller than most macromolecules in a cell. The high-resolution TEM (HRTEM) image (Figure 1d) shows that the GQDs exhibit high crystallinity with a lattice spacing of 0.24 nm, corresponding to (1120) lattice fringes of graphene. The atomic force microscopy (AFM) image reveals that the topographic height of a GQD is ~1 nm, in agreement with the thickness of single-layer graphene (Figure 1e). GQDs made here are a single-atom-thick carbon sheet with good crystallinity and a diameter of ~2.2 nm. They are distinct from

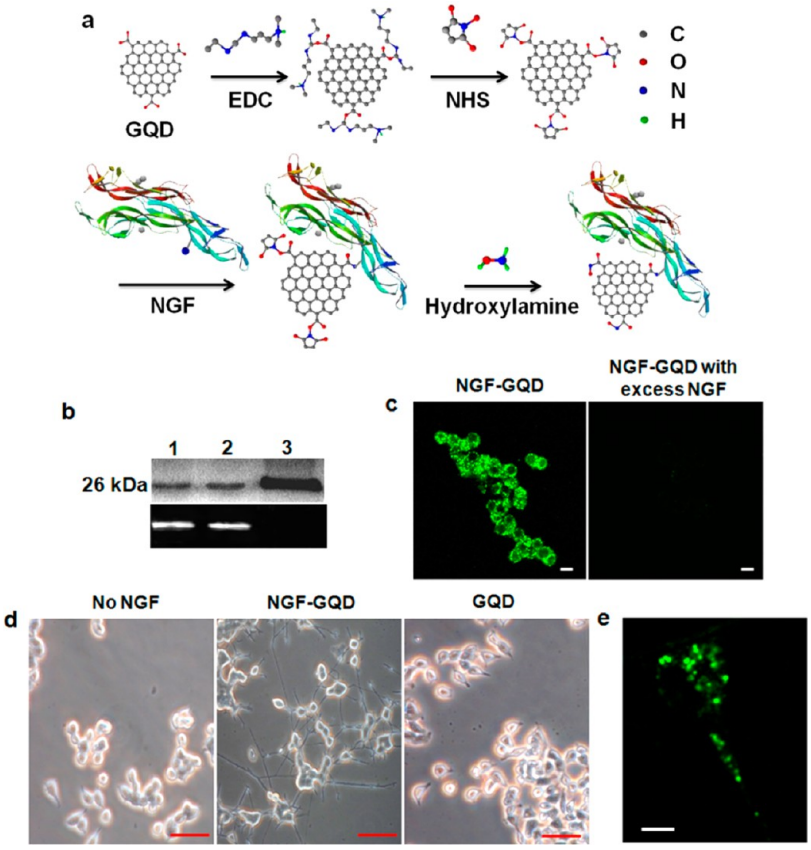

Figure 2. NGF-GQD is biologically functional. (a) Schematic illustration of conjugating a GQD with NGF. (b) Gel electrophoresis of NGF-GQD (lane 1), FITC-NGF (lane 2), and NGF (lane 3). (c) Fluorescence images of living PC12 cells incubated with 200 ng/mL NGF-GQDs (left) or NGF-GQDs together with 20 μg/mL free NGF (right) for 15 min. (d) Representative phase-contrast images of PC12 cells after 2-day incubation without (left) or with 200 ng/mL NGF-GQDs (middle) or with GQDs (right). Scale bar = 50 μm. (e) Distribution of NGF-GQDs in PC12 cells differentiated by 200 ng/mL NGF-GQDs for 24 h. Scale bar = 5 μm.

the previously reported fluorescent carbon dots, which are carbon spheres (<10 nm) consisting of an amorphous to nanocrystalline core.[27] Figure 1f presents the Raman spectrum of the GQDs, which exhibits two characteristic peaks, at 1351 and 1585 cm^{-1}, corresponding to the D and G band of graphene, respectively. The I_D/I_G ratio (*ca.* 0.9) is similar to that of graphene oxides (GO).[28] Confirming the previous reports, we also show that the GQDs are highly biocompatible; specifically, a dose as high as 100 μg/mL does not introduce obvious cytotoxicity (Supporting Information, Figure S1).

Figure 2 illustrates a general route for functionalization of a protein or peptide with a GQD using nerve growth factor (NGF) as an example. First, 1-ethyl-3-(3-dimethylaminopropyl)carbodiimide hydrochloride (EDC) is applied to react with the carboxyl groups on the edge of the GQD, forming an amine-reactive *O*-acylisourea intermediate. This intermediate is unstable due to its susceptibility to hydrolysis. Therefore, *N*-hydroxysuccinimide (NHS) is subsequently added to convert it to an amine-reactive NHS ester. The NHS ester modified GQD can then covalently react with the amine groups universally available in most proteins and peptides. Lastly, hydroxylamine is added to convert the remaining NHS esters into hydroxamic acids, thereby quenching the reaction. By the way, GQD is conjugated with a molecule without a cross-linker in between, which may otherwise interfere with the functionalities of the molecule. This zero-length cross-linker strategy has been previously used to conjugate PEG-amine to the carboxylic groups on graphene oxide.[29] Using this facile bioconjugation method, we verified that all the tested proteins can be successfully coupled with GQDs, including neuropeptide Y, bovine serum albumin, immunoglobulin G, concanavalin A, insulin, and NGF. As shown in Figure S2 (Supporting Information), each protein-GQD derivative gives only a single band from gel electrophoresis in both the bright-field and fluorescent images, confirming that no aggregations between GQD derivatives form.

To further prove that GQDs can serve as universal fluoro-tags, we carefully evaluated NGF-conjugated GQDs (NGF-GQD). As shown in Figure 2b, the electrophoretic mobility of NGF-GQDs is similar to that of FITC (~0.4 kDa)-labeled NGF and native NGF (~26 kDa), indicating that the attachment of GQD does not significantly increase the overall weight of the conjugate and the GQD does not pair with multiple NGF

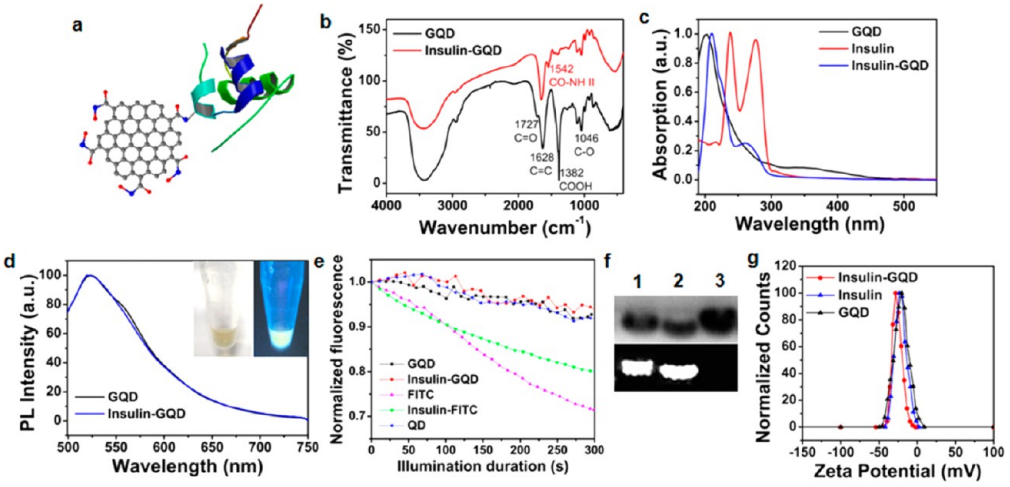

Figure 3. Characterization of insulin-GQD conjugates. (a) Illustration of insulin-GQD. (b) FTIR spectra of GQD and insulin-GQD. (c) UV−vis absorption spectra of GQD, insulin, and insulin-GQD. (d) Photoluminescence (PL) spectra of GQD and insulin-GQD. The excitation wavelength is 488 nm. Inset shows the optical and fluorescent images of an insulin-GQD aqueous suspension. (e) Photobleaching profile of GQD, insulin-GQD, FITC, insulin-FITC, and CdTe-QD. (f) Gel electrophoresis of insulin-GQD (lane 1), insulin-FITC (lane 2), and insulin (lane 3). (g) Zeta potential of insulin, GQD, and insulin-GQD at pH 7.

molecules. In contrast to the large semiconductor QDs, which usually cannot realize one-to-one conjugation without carefully designed and controlled conjugation strategies, GQDs are comparable with small fluorophores such as FITC, yet much more stable.

To show that the conjugated NGF retains its functionality, we then examined the ability of NGF-GQDs to bind specifically with NGF receptors abundantly expressed in neuroendocrine PC12 cells. As demonstrated by the confocal fluorescence image shown in Figure 2c, PC12 cells incubated with 200 ng/mL NGF-GQD for 15 min show numerous bright fluorescent puncta both on the cell membrane and in the cytosol, presumably resulting from the binding of NGF-GQDs with NGF receptors on the cell membrane and rapid internalization of the activated receptor complex.[30,31] In the control experiment, when excess free NGF molecules were added together, NGF-GQD staining was completely eliminated due to competitive inhibition (Figure 2c). This unambiguously demonstrates the specific recognition between NGF-GQDs and the NGF receptors. Furthermore, Figure 2d shows that NGF-GQDs were able to stimulate neurite outgrowth in PC12 cells, whereas bare GQDs could not, verifying that the NGF-GQD conjugate is capable of activating the NGF signaling pathway. In the neuronal differentiated PC12 cells by NGF-GQDs, the fluorescent NGF-GQDs were observed to distribute in the cell body and along the neurites (Figure 2e), similar to the previous report using NGF-functionalized CdSe/ZnS QDs.[5]

Thus far, we have demonstrated the potential of GQDs as universal small fluorophores that can be conveniently and covalently tagged with any amine-bearing biomolecule without impairing its functionalities. As a more careful case study and a proof-of-concept demonstration of using GQDs for biological studies, we further sought to demonstrate the use of insulin-GQDs to label and track the dynamics of insulin receptors in adipocytes (fat cells) in a physiological context for the first time.

The Fourier transform infrared (FTIR) spectrum (Figure 3b) reveals the existence of C═O (1727 cm^{-1}), C═C (1628 cm^{-1}), COOH (1382 cm^{-1}), and C−O (1046 cm^{-1}) functional groups in the GQD. In the insulin-GQD conjugates, the COOH peak diminishes, while a new peak appears at 1542 cm^{-1} corresponding to the formation of an amide linkage, confirming that the COOH groups are used to form a conjugation with insulin. As shown in the UV−vis spectra (Figure 3c), the GQD has an absorption peak at 202 nm, while insulin exhibits absorption peaks at 237 and 276 nm. In comparison, the insulin-GQD has an absorption maximum at 209 nm with two shoulders at 224 and 267 nm, further verifying the successful conjugation of insulin with the GQD.

Both bare GQDs and insulin-GQDs in PBS solution are light yellow under daylight and give olivine fluorescence upon excitation at 488 nm (Figure 3d). The photoluminescence spectra of GQDs and insulin-GQDs are similar, with an emission peak at ~520 nm (Figure 3d), suggesting that the photoluminescence property of GQDs changes little after the conjugation. It is, however, notable that the emission peak of GQDs is wide as compared to semiconductor QDs. This would increase crosstalk in multicolor imaging. For such experiments, better control of the GQD homogeneity (both size and surface chemistry) is desired to narrow the emission peak. As shown in Figure 3e, the fluorescence of insulin-GQDs and GQDs only gradually declines over time due to photobleaching (1.4%/min), whereas a precipitous decay in fluorescence is

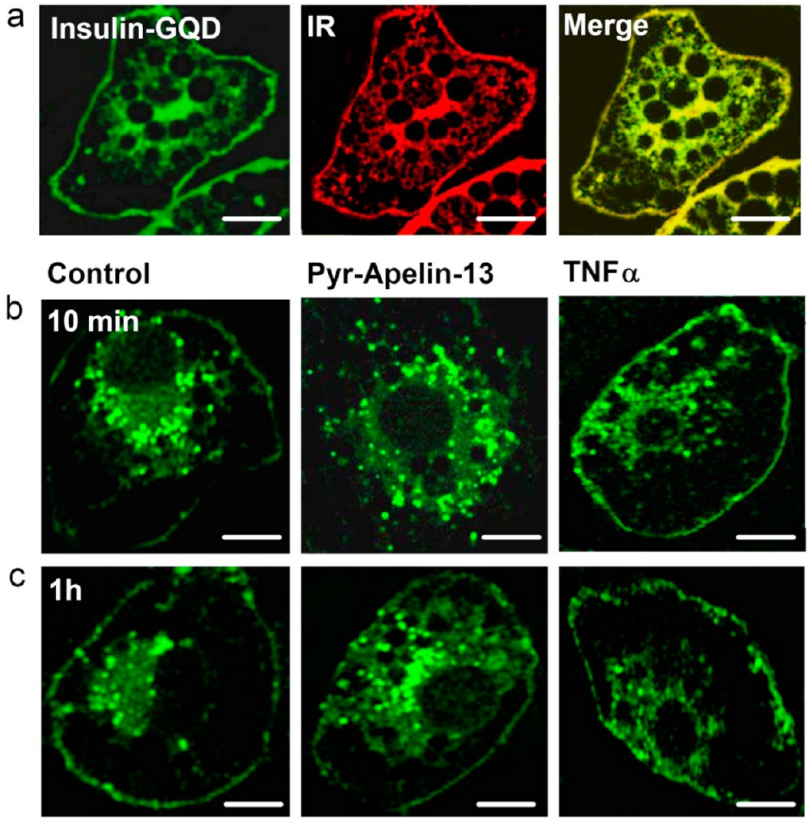

Figure 4. Confocal fluorescence imaging of an insulin receptor in 3T3-L1 adipocytes. (a) Representative confocal fluorescence images of a fixed and permeabilized adipocyte labeled with insulin-GQDs (green, left) or with antibodies against insulin receptor β subunit followed by Atto647 NHS-conjugated secondary antibodies (red, middle). The merged image is shown on the right. Scale bar = 10 μm. (b, c) Confocal fluorescence images showing the cellular distribution of insulin receptors in control and pyr-apelin-13 (1 μM)- or TNFα (50 ng/mL)-treated adipocytes after (b) 10 min or (c) 1 h incubation with insulin-GQDs.

observed for FITC and FITC-labeled insulin (insulin-FITC). The photobleaching rate of GQDs is similar to that of CdTe QDs, although other types of semiconductor QDs may be more stable to some extent. Thus, GQDs can be considered as a photostable label suitable for fluorescence tracking experiments. As shown in Figure 3f, insulin-GQD conjugates show similar gel mobility to that of insulin-FITC and insulin itself (~6 kDa), implying one-to-one pairing between insulin and GQDs and that the GQD tag does not significantly affect the charge state of insulin. The latter is also confirmed by the observation that the zeta potential of insulin-GQDs (-26.0 ± 6.07 mV, $n = 3$) is similar to that of insulin (-21.1 ± 7.3 mV, $n = 3$) and GQDs (-20.3 ± 7.6 mV, $n = 3$) (Figure 3g). The desired one-to-one pairing between GQDs and insulin can be attributed to the electrostatic repulsion between negatively charged insulin molecules and the fact that the size of a GQD is comparable to the Debye charge screening length in physiological conditions. In addition, insulin-GQD conjugates have also been purified by gel filtration using a desalting column (10-PD, Ge Healthcare), which gives a single band with gel mobility similar to insulin (Supporting Information, Figure S3), proving the absence of physisorption. We further verified that fluorescent insulin-GQD conjugates cannot be formed in the absence of EDC/NHS linkers, implying that no nonspecific interactions exist between insulin and GQDs (Supporting Information, Figure S4).

Insulin signaling, mediated by insulin receptors, plays a central role in the regulation of cellular glucose metabolism as well as other functions. Impaired response to insulin is the hallmark of diabetes, while excessive insulin activity is correlated with cancers.[32,33] Binding between insulin and insulin receptors at the plasma membrane triggers receptor internalization and recycling.[34,35] The inefficiency of such receptor turnover is associated with insulin resistance, which is a notorious cause of many diseases (*e.g.*, type 2 diabetes).[36] Although revealing the trafficking dynamics of insulin receptors is of obvious importance, it remains challenging and poorly studied partly due to the lack of labeling methods for live-cell imaging. Organic fluorophores such as FITC are not suitable for long-term real-time imaging experiments due to severe photobleaching. On the other hand, semiconductor quantum dots (~500 kDa) are much larger than insulin (~6 kDa) and may significantly alter the receptor dynamics, leading to artifacts. GQDs are most suitable here due to their good quantum yield, excellent photostability, biocompatibility, and small size.

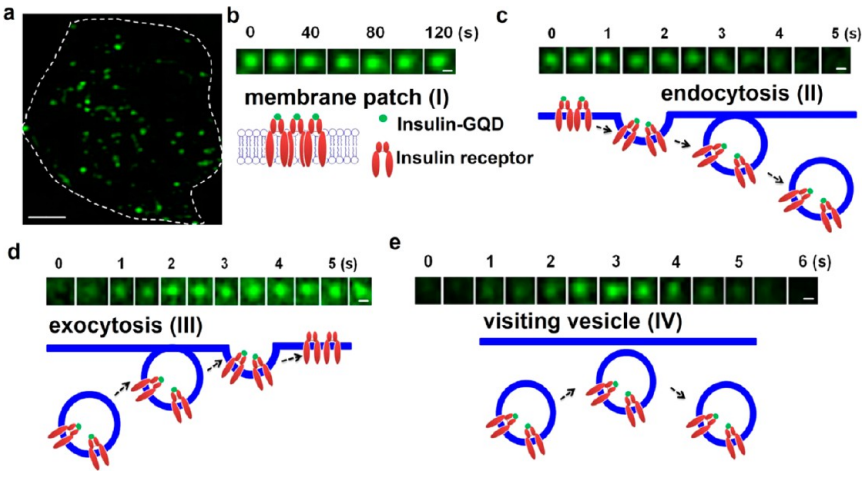

Figure 5. Tracking the dynamics of insulin receptors in living adipocytes using TIRFM. (a) Typical TIRFM image of a 3T3-L1 adipocyte after 1 h incubation of insulin-GQDs. Scale bar = 5 μm. (b) Membrane patch consisting of insulin-GQD/insulin receptor clusters (type I). (c) Endocytosis of fluorescent membrane patches into a vesicle (type II). (d) Exocytosis of a vesicle containing insulin-GQD/insulin receptor complexes (type III). (e) Transient approaching and retrieval of insulin-GQD/insulin receptor containing vesicle (type IV). Scale bars = 0.2 μm.

Previous studies have provided evidence that TNFα (a pro-inflammatory factor) induces insulin resistance[37,38] and apelin (a novel signaling peptide expressed in various cell types including adipocytes) is able to improve insulin sensitivity.[39−41] However, the underlying mechanisms of how these cytokines act, particularly their influences on insulin receptors, are still elusive.

As observed by confocal fluorescence imaging (Figure 4a), incubation (1 h) of insulin-GQDs with fixed and permeablized 3T3-L1 adipocytes (cell culturing is detailed in the Supporting Information) results in cellular staining perfectly co-localized with immunostaining using insulin receptor-specific primary antibodies and fluorophore (Atto647 NHS)-conjugated secondary antibodies, indicating the ability of insulin-GQDs to specifically label insulin receptors and reveal their cellular distribution. As shown, insulin receptors abundantly reside in the cell membrane and also scatter in the cytosol.

Confocal analyses of insulin receptor localization were then performed with short-time incubation (10 min) of insulin-GQDs with live adipocytes (control or pretreated with apelin or TNFα) followed by cell fixation. In control cells, most insulin receptors are found in the cell interior, while a small fraction of them remain on the plasma membrane, indicating that the majority of insulin receptors are quickly (within 10 min) internalized (or endocytosed) into the cytoplasm upon binding with insulin-GQDs (Figure 4b). In comparison, insulin-stimulated receptor internalization is largely enhanced by apelin treatment but inhibited by TNFα (Figure 4b). Evidently, apelin and TNFα regulate insulin receptor trafficking oppositely, consistent with their effects on insulin sensitivity. As the insulin-GQD incubation time is extended to 1 h, membrane staining with GQDs reappears for control and apelin-treated cells, suggesting the recycling of insulin receptors back to the plasma membrane (Figure 4c).

We further investigated the dynamic trafficking of insulin receptors using total internal reflection fluorescence microscopy, which evanescently and selectively illuminates the thin plasmalemmal region (<200 nm thick). TIRFM is powerful in revealing the molecular events taking place in close vicinity to the cell membrane with minimal interference from the cell interior and with a higher temporal resolution than confocal microscopy.[42]

After preincubating adipocytes with insulin-GQDs to allow endocytosis and exocytosis of insulin receptors, time-lapse images were taken under TIRFM for 2 min with a sampling frequency of 2 Hz. Small discrete clusters of GQDs are observed under TIRFM (Figure 5a), presumably due to the insulin-GQD/insulin receptor complex containing vesicles immediately underneath the plasma membrane or membrane microdomains enriched with the receptor complexes. These GQD-enlightened clusters undertake constant lateral movement parallel to the cell membrane and vertical movement between the inner cytosol and the plasmalemmal region, as indicated by the appearance, disappearance, and fluctuation in GQD fluorescence. On the basis of real-time tracking of individual clusters during the 2 min imaging period, four subpopulations can be clearly identified including (type I) membrane patches consisting of insulin-GQD/insulin receptor clusters characterized by constant fluorescence and slow mobility (Figure 5b); (type II) fluorescent membrane patches endocytosed into vesicles characterized by gradual dimming and final disappearance of fluorescence (Figure 5c); (type III) exocytosis (fusion with the membrane) of the vesicles containing insulin-GQD/insulin receptor complexes characterized by the appearance and gradually brightened fluorescence (Figure 5d); and

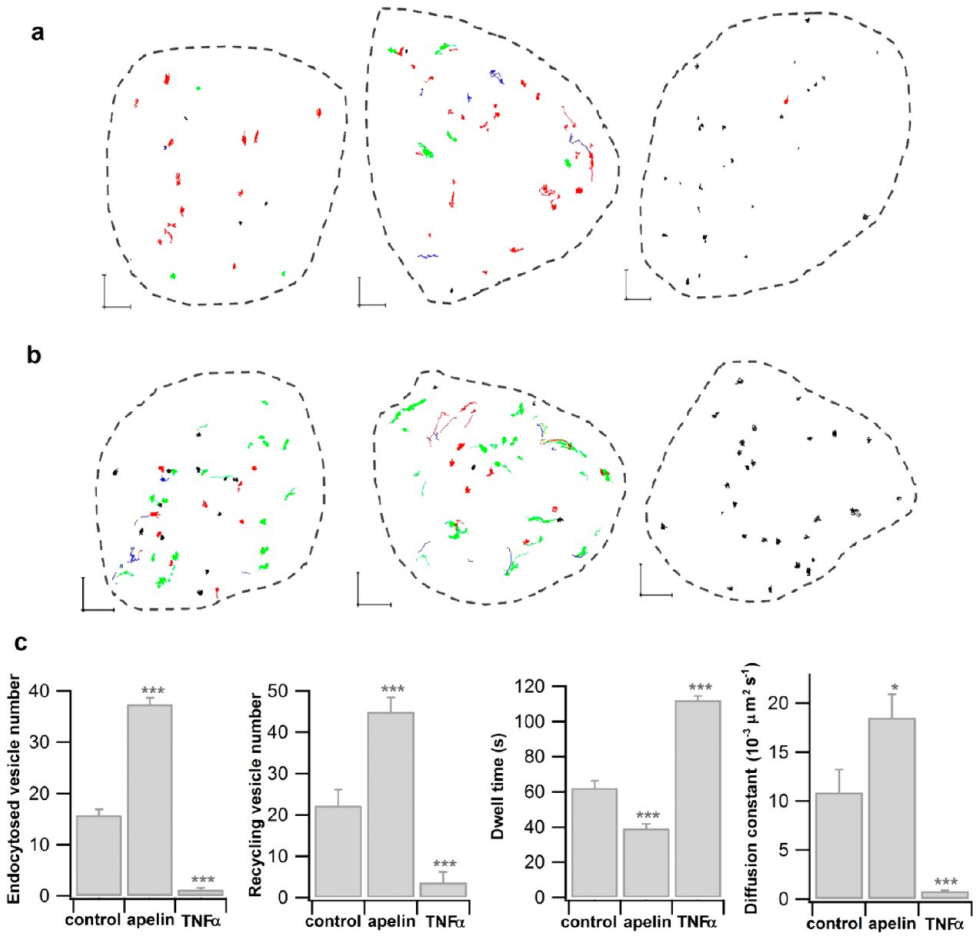

Figure 6. Effects of apelin and TNFα on insulin receptor trafficking dynamics. (a, b) Individual trajectories of GQD-cluster movement are shown in a control cell (left), an apelin-treated cell (middle), and a TNFα-treated cell (right) after (a) 10 min or (b) 1 h incubation with insulin-GQDs. The cell contours are illustrated by dashed lines. Black, red, green, and blue traces represent the trajectories for membrane patches (type I), endocytotic event (type II), exocytotic event (type III), and visiting vesicles (type IV), respectively. (c) Statistics of the endocytosed vesicle number per cell after 10 min insulin-GQD incubation, the recycling (endocytosed and exocytosed) vesicle number per cell, dwell time, and diffusion constant after 1 h incubation in control cells (764 tracks, 12 cells), apelin-treated cells (832 tracks, 12 cells), and TNFα-treated cells (769 tracks, 12 cells). The error bars indicate the standard errors. Student's *t*-test: ***$p < 0.001$, *$p < 0.05$ *vs* control.

(type IV) transient approaching and retrieval of insulin-GQD/insulin receptor containing vesicles (Figure 5e). As shown by mean square displacement analyses (Supporting Information, Figure S5), type I clusters mostly undertake confined and inactive movement, whereas some clusters in types II–IV can undertake fast directional movement parallel to the cell membrane.

Figure 6a shows TIRFM imaging of a representative adipocyte right after a 10 min incubation with insulin-GQDs, without or pretreated with apelin or TNFα. The motion trajectories of the four types of GQD clusters are labeled with different colors. As seen from Figure 6a and c, the endocytosis events (type II) dominate in the control cell, indicating that the dynamics of internationalization of activated receptors is on the order of minutes, while in the apelin-treated cells, both endocytosis and exocytosis (type III) events are greatly enhanced, suggesting facilitated receptor turnover. In contrast, the receptor turnover is essentially inhibited in the TNFα-treated cells, as evidenced by the observation that the patches of insulin-GQDs remain bound on the membrane (type I). Figure 6b depicts representative adipocytes after a longer incubation time (1 h) with insulin-GQDs (also see Video S1 for a control cell in the Supporting Information). As seen from Figure 6b and c, the total number of recycling vesicles (exocytotic and endocytotic) is largely increased by apelin and essentially eliminated by TNFα. This demonstrates the opposite regulation of these two cytokines in insulin receptor turnover, consistent with the confocal observations. In endocrine cells, the turnover rate of secretory vesicles is positively correlated with their lateral diffusion constant and negatively correlated with their dwell-time in the subplasmalemmal region.[42] In line with this, apelin greatly reduces the dwell-time and enhances the diffusion constant of GQD-lightened insulin receptor clusters, whereas TNFα does the opposite. Insulin binding with its receptor on the cell membrane triggers translocation of GLUT-4 glucose transporters to the plasma

membrane for subsequent uptake of glucose, and the activated insulin receptors will be internalized and recycled for the next rounds of action.[38] Our results suggest that the known ability of TNFα to induce insulin resistance for glucose metabolism can be, at least in part, attributed to its inhibition of insulin receptor turnover (thus sustaining the action of the receptor). Similarly, our results also imply that the known ability of apelin to enhance insulin sensitivity for glucose metabolism can be attributed to its stimulation of insulin receptor dynamics.

CONCLUSIONS

In summary, we have demonstrated the use of GQDs as universal and excellent fluoro-tags to specifically label and track molecular targets, owing to their stable photoluminescence, small size, ease of functionalization, biocompatibility, good solubility, and chemical inertness. The internalization, trafficking, and recycling of insulin receptors in adipocytes have been monitored in real-time using insulin-conjugated GQDs. We reveal for the first time that the insulin receptor dynamics are stimulated by apelin and inhibited by TNFα, providing evidence for the molecular mechanisms underlying the regulation of these cytokines in insulin sensitivity. This study demonstrates the great potentials of GQDs in live-cell imaging, particularly for investigating dynamic cellular processes. It adds a new dimension to the application of graphene materials for nanomedicine[43,44] as well as the application of nanotechnologies to resolve dynamic cell functions.[45]

METHODS

GQD Synthesis and Characterization. The precursor, carbon black (0.2 g, Vulcan CX-72, Cabot Corporation), was refluxed with nitric acid (50 mL, 6 M) for 24 h.[26] After centrifugation (2770*g*, 10 min), the supernatant was heated to yield a reddish-brown powder, which was then resuspended in DI water and filtered through a 0.22 μm microporous membrane. The colloidal solution was further ultrafiltered through a centrifugal filter device using a filtering membrane with a cutoff molecular weight of 3 kDa (Amicon Ultra-4, Millipore) for 40 min. The strongly fluorescent GQDs were obtained in the filtrate. TEM was conducted on a JEOL (JEM 2010) electron microscope at an acceleration voltage of 200 kV. GQDs were also characterized with tapping-mode AFM (MFP-3D, Asylum Research) using an NCH20 tip (silicon cantilever, Nanoworld). Raman spectra were recorded at ambient temperature on a WITeck CRM200 confocal microscopy Raman system with a 633 nm laser.

GQD Bioconjugation. The GQD solution (0.5 mg/mL) was first mixed with 1-ethyl-3-(3-dimethylaminopropyl)carbodiimide hydrochloride (10 mM) and *N*-hydroxysuccinimide (10 mM) for 15 min. NGF (~26 kDa) or insulin (~6 kDa, 0.1 mg/mL) was subsequently added into the above mixture for 4 h at room temperature. The reaction was quenched by adding hydroxylamine (10 mM). The obtained samples were ultrafiltered three times (centrifuging at 7500*g* for 20 min) with PBS to remove free unconjugated GQDs. Filters with a molecular weight cutoff (MWCO) of 10 and 3 kDa were used for purifying NGF-GQDs and insulin-GQDs, respectively. The conjugated GQD samples were then separated in the 10−12% SDS polyacrylamide gels at 140 V for 40 min and imaged with a gel imaging system (ProXPRESS 2D, Pekin Elmer) to confirm the successful bioconjugation.

FTIR was performed with a Perkin-Elmer FT-IR Spectrum GX. Spectroscopic properties of GQD samples were characterized by a UV−vis spectrophotometer (Nanodrop 2200c, Thermo Scientific) and a fluorospectrometer (Nanodrop 3300). The zeta potential of GQD samples was measured using a Zetasizer 3000 (Malvern Instruments).

Confocal Fluorescence Imaging. PC12 cells were incubated with NGF-GQDs (200 ng/mL) for 15 min or 24 h, then washed. For the competitive assay, excess free NGF (20 μg/mL) was added to the PC12 cells for 10 min, followed by the addition of NGF-GQDs. 3T3-L1 adipocytes were untreated or pretreated with TNFα (50 ng/mL) or pyr-apelin-13 (1 μM) for 1 h at 37 °C, followed by incubation with insulin-GQDs (10 μg/mL) for 10 min or 1 h. Adipocytes were washed, fixed with 4% formaldehyde in ice-cold PBS, and imaged using a confocal microscope (Zeiss LSM 510) with a 63× oil objective and a 488 nm laser. For the immunostaining experiment, after 3T3-L1 adipocytes were fixed, insulin receptors were stained in PBS-Tween solution with specific rabbit anti-insulin receptor IgG (C-terminal of β-subunit, Santa Cruz Biotechnology) overnight followed by incubation with anti-rabbit IgG conjugated with Atto647 NHS (Sigma) and 10 μg/mL insulin-GQDs for 1 h.

Total Internal Reflection Fluorescence Microscopy. The adipocytes were incubated with insulin-GQDs for 10 min or 1 h at 37 °C prior to imaging. The cells were washed and incubated in a bath solution (150 mM NaCl, 5 mM KCl, 1.1 mM $MgCl_2$, 2.6 mM $CaCl_2$, 10 mM HEPES, and 10 mM glucose, pH 7.4) during imaging. Time-lapse images (241 frames, 0.5 s/frame) were recorded at 37 °C using an inverted TIRFM microscope (Axiovert 200, Carl Zeiss) with a 100× oil objective (NA = 1.45) and a charge-coupled device camera (CCD, pixel size = 0.248 μm). The trajectories of the clusters of GQD-labeled receptor complex were individually and manually tracked using ImageJ (National Institute of Health, Wayne Rasband, USA) and analyzed by Igor routines (WaveMetrics, Lake Oswego, OR, USA).

Conflict of Interest: The authors declare no competing financial interest.

Acknowledgment. We thank the support from the Ministry of Education of Singapore under an AcRF Tier 2 grant (MOE2011-T2-2-010) and the Agency for Science, Technology and Research (A*STAR) under a SERC grant (102 170 0142).

Supporting Information Available: Figures S1−S5, video S1, and detailed methods. This material is available free of charge *via* the Internet at http://pubs.acs.org.

REFERENCES AND NOTES

1. Michalet, X.; Pinaud, F. F.; Bentolila, L. A.; Tsay, J. M.; Doose, S.; Li, J. J.; Sundaresan, G.; Wu, A. M.; Gambhir, S. S.; Weiss, S. Quantum Dots for Live Cells, *in Vivo* Imaging, and Diagnostics. *Science* **2005**, *307*, 538–544.
2. Zhang, J.; Campbell, R. E.; Ting, A. Y.; Tsien, R. Y. Creating New Fluorescent Probes for Cell Biology. *Nat. Rev. Mol. Cell Biol.* **2002**, *3*, 906–918.
3. Lukinavičius, G.; Umezawa, K.; Olivier, N.; Honigmann, A.; Yang, G.; Plass, T.; Mueller, V.; Reymond, L.; Corrêa, I. R., Jr.; Luo, Z.-G.; *et al*. A Near-Infrared Fluorophore for Live-Cell Super-Resolution Microscopy of Cellular Proteins. *Nat. Chem.* **2013**, *5*, 132–139.
4. Resch-Genger, U.; Grabolle, M.; Cavaliere-Jaricot, S.; Nitschke, R.; Nann, T. Quantum Dots *versus* Organic Dyes as Fluorescent Labels. *Nat. Methods* **2008**, *5*, 763–775.
5. Vu, T. Q.; Maddipati, R.; Blute, T. A.; Nehilla, B. J.; Nusblat, L.; Desai, T. A. Peptide-Conjugated Quantum Dots Activate Neuronal Receptors and Initiate Downstream Signaling of Neurite Growth. *Nano Lett.* **2005**, *5*, 603–607.
6. Jiang, S.; Liu, A. P.; Duan, H. W.; Soo, J.; Chen, P. Labeling and Tracking P2 Purinergic Receptors in Living Cells Using ATP-Conjugated Quantum Dots. *Adv. Funct. Mater.* **2011**, *21*, 2776–2780.

7. Pinaud, F.; Clarke, S.; Sittner, A.; Dahan, M. Probing Cellular Events, One Quantum Dot at a Time. *Nat. Methods* **2010**, *7*, 275–285.
8. Pan, D. Y.; Zhang, J. C.; Li, Z.; Wu, M. H. Hydrothermal Route for Cutting Graphene Sheets into Blue-Luminescent Graphene Quantum Dots. *Adv. Mater.* **2010**, *22*, 734–738.
9. Jin, S. H.; Kim, D. H.; Jun, G. H.; Hong, S. H.; Jeon, S. Tuning the Photoluminescence of Graphene Quantum Dots through the Charge Transfer Effect of Functional Groups. *ACS Nano* **2012**, *7*, 1239–1245.
10. Tetsuka, H.; Asahi, R.; Nagoya, A.; Okamoto, K.; Tajima, I.; Ohta, R.; Okamoto, A. Optically Tunable Amino-Functionalized Graphene Quantum Dots. *Adv. Mater.* **2012**, *24*, 5333–5338.
11. Zhuo, S. J.; Shao, M. W.; Lee, S. T. Upconversion and Downconversion Fluorescent Graphene Quantum Dots: Ultrasonic Preparation and Photocatalysis. *ACS Nano* **2012**, *6*, 1059–1064.
12. Shen, J.; Zhu, Y.; Yang, X.; Li, C. Graphene Quantum Dots: Emergent Nanolights for Bioimaging, Sensors, Catalysis and Photovoltaic Devices. *Chem. Commun.* **2012**, *48*, 3686–3699.
13. Dong, Y. Q.; Shao, J. W.; Chen, C. Q.; Li, H.; Wang, R. X.; Chi, Y. W.; Lin, X. M.; Chen, G. N. Blue Luminescent Graphene Quantum Dots and Graphene Oxide Prepared by Tuning the Carbonization Degree of Citric Acid. *Carbon* **2012**, *50*, 4738–4743.
14. Lin, L. X.; Zhang, S. W. Creating High Yield Water Soluble Luminescent Graphene Quantum Dots *via* Exfoliating and Disintegrating Carbon Nanotubes and Graphite Flakes. *Chem. Commun.* **2012**, *48*, 10177–10179.
15. Zhu, S. J.; Zhang, J. H.; Liu, X.; Li, B.; Wang, X. F.; Tang, S. J.; Meng, Q. N.; Li, Y. F.; Shi, C.; Hu, R.; *et al*. Graphene Quantum Dots with Controllable Surface Oxidation, Tunable Fluorescence and Up-Conversion Emission. *RSC Adv.* **2012**, *2*, 2717–2720.
16. Sun, H. J.; Wu, L.; Gao, N.; Ren, J. S.; Qu, X. G. Improvement of Photoluminescence of Graphene Quantum Dots with a Biocompatible Photochemical Reduction Pathway and Its Bioimaging Application. *ACS Appl. Mater. Interfaces* **2013**, *5*, 1174–1179.
17. Liu, J. J.; Zhang, X. L.; Cong, Z. X.; Chen, Z. T.; Yang, H. H.; Chen, G. N. Glutathione-Functionalized Graphene Quantum Dots as Selective Fluorescent Probes for Phosphate-Containing Metabolites. *Nanoscale* **2013**, *5*, 1810–1815.
18. Tang, L.; Ji, R.; Cao, X.; Lin, J.; Jiang, H.; Li, X.; Teng, K. S.; Luk, C. M.; Zeng, S.; Hao, J.; *et al*. Deep Ultraviolet Photoluminescence of Water-Soluble Self-Passivated Graphene Quantum Dots. *ACS Nano* **2012**, *6*, 5102–5110.
19. Zhang, Z. P.; Zhang, J.; Chen, N.; Qu, L. T. Graphene Quantum Dots: An Emerging Material for Energy-Related Applications and Beyond. *Energy Environ. Sci.* **2012**, *5*, 8869–8890.
20. Yan, X.; Li, B.; Li, L.-s..Colloidal Graphene Quantum Dots with Well-Defined Structures. *Acc. Chem. Res.*, DOI: 10.1021/ar300137p.
21. Zhu, S. J.; Zhang, J. H.; Qiao, C. Y.; Tang, S. J.; Li, Y. F.; Yuan, W. J.; Li, B.; Tian, L.; Liu, F.; Hu, R.; *et al*. Strongly Green-Photoluminescent Graphene Quantum Dots for Bioimaging Applications. *Chem. Commun.* **2011**, *47*, 6858–6860.
22. Peng, J.; Gao, W.; Gupta, B. K.; Liu, Z.; Romero-Aburto, R.; Ge, L.; Song, L.; Alemany, L. B.; Zhan, X.; Gao, G.; *et al*. Graphene Quantum Dots Derived from Carbon Fibers. *Nano Lett.* **2012**, *12*, 844–849.
23. Zhu, S. J.; Zhang, J. H.; Tang, S. J.; Qiao, C. Y.; Wang, L.; Wang, H. Y.; Liu, X.; Li, B.; Li, Y. F.; Yu, W. L.; *et al*. Surface Chemistry Routes to Modulate the Photoluminescence of Graphene Quantum Dots: From Fluorescence Mechanism to Up-Conversion Bioimaging Applications. *Adv. Funct. Mater.* **2012**, *22*, 4732–4740.
24. Pan, D. Y.; Guo, L.; Zhang, J. C.; Xi, C.; Xue, Q.; Huang, H.; Li, J. H.; Zhang, Z. W.; Yu, W. J.; Chen, Z. W.; *et al*. Cutting Sp(2) Clusters in Graphene Sheets into Colloidal Graphene Quantum Dots with Strong Green Fluorescence. *J. Mater. Chem.* **2012**, *22*, 3314–3318.
25. Sun, X. M.; Liu, Z.; Welsher, K.; Robinson, J. T.; Goodwin, A.; Zaric, S.; Dai, H. J. Nano-Graphene Oxide for Cellular Imaging and Drug Delivery. *Nano Res.* **2008**, *1*, 203–212.
26. Dong, Y. Q.; Chen, C. Q.; Zheng, X. T.; Gao, L. L.; Cui, Z. M.; Yang, H. B.; Guo, C. X.; Chi, Y. W.; Li, C. M. One-Step and High Yield Simultaneous Preparation of Single- and Multi-Layer Graphene Quantum Dots from Cx-72 Carbon Black. *J. Mater. Chem.* **2012**, *22*, 8764–8766.
27. Baker, S. N.; Baker, G. A. Luminescent Carbon Nanodots: Emergent Nanolights. *Angew. Chem., Int. Ed.* **2010**, *49*, 6726–6744.
28. Gao, W.; Alemany, L. B.; Ci, L. J.; Ajayan, P. M. New Insights into the Structure and Reduction of Graphite Oxide. *Nat. Chem.* **2009**, *1*, 403–408.
29. Liu, Z.; Robinson, J. T.; Sun, X. M.; Dai, H. J. Pegylated Nanographene Oxide for Delivery of Water-Insoluble Cancer Drugs. *J. Am. Chem. Soc.* **2008**, *130*, 10876–10877.
30. Cui, B. X.; Wu, C. B.; Chen, L.; Ramirez, A.; Bearer, E. L.; Li, W. P.; Mobley, W. C.; Chu, S. One at a Time, Live Tracking of NGF Axonal Transport Using Quantum Dots. *Proc. Natl. Acad. Sci. U.S.A.* **2007**, *104*, 13666–13671.
31. Rajan, S. S.; Liu, H. Y.; Vu, T. Q. Ligand-Bound Quantum Dot Probes for Studying the Molecular Scale Dynamics of Receptor Endocytic Trafficking in Live Cells. *ACS Nano* **2008**, *2*, 1153–1166.
32. Saltiel, A. R.; Kahn, C. R. Insulin Signalling and the Regulation of Glucose and Lipid Metabolism. *Nature* **2001**, *414*, 799–806.
33. Pandini, G.; Frasca, F.; Mineo, R.; Sciacca, L.; Vigneri, R.; Belfiore, A. Insulin/Insulin-Like Growth Factor I Hybrid Receptors Have Different Biological Characteristics Depending on the Insulin Receptor Isoform Involved. *J. Biol. Chem.* **2002**, *277*, 39684–39695.
34. Marshall, S. Kinetics of Insulin-Receptor Internalization and Recycling in Adipocytes - Shunting of Receptors to a Degradative Pathway by Inhibitors of Recycling. *J. Biol. Chem.* **1985**, *260*, 4136–4144.
35. Fagerholm, S.; Örtegren, U.; Karlsson, M.; Ruishalme, I.; Strålfors, P. Rapid Insulin-Dependent Endocytosis of the Insulin Receptor by Caveolae in Primary Adipocytes. *PLoS one* **2009**, *4*, e5985.
36. Trischitta, V.; Reaven, G. M. Evidence of a Defect in Insulin-Receptor Recycling in Adipocytes from Older Rats. *Am. J. Physiol.* **1988**, *254*, E39–E44.
37. Hotamisligil, G. S.; Peraldi, P.; Budavari, A.; Ellis, R.; White, M. F.; Spiegelman, B. M. IRS-1-Mediated Inhibition of Insulin Receptor Tyrosine Kinase Activity in TNF-Alpha- and Obesity-Induced Insulin Resistance. *Science* **1996**, *271*, 665–668.
38. Inokuchi, J. Membrane Microdomains and Insulin Resistance. *FEBS Lett.* **2010**, *584*, 1864–1871.
39. Zou, C. H.; Shao, J. H. Role of Adipocytokines in Obesity-Associated Insulin Resistance. *J. Nutr. Biochem.* **2008**, *19*, 277–286.
40. Zhu, S. M.; Sun, F.; Li, W. J.; Cao, Y. J.; Wang, C.; Wang, Y. B.; Liang, D.; Zhang, R. Q.; Zhang, S. W.; Wang, H. C.; *et al*. Apelin Stimulates Glucose Uptake through the PI3K/Akt Pathway and Improves Insulin Resistance in 3T3-L1 Adipocytes. *Mol. Cell. Biochem.* **2011**, *353*, 305–313.
41. Castan-laurell, I.; Dray, C.; Knauft, C.; Kunduzova, O.; Valet, P. Apelin, a Promising Target for Type 2 Diabetes Treatment? *Trends Endocrinol. Metab.* **2012**, *23*, 234–241.
42. Zhang, J.; Xue, R. H.; Ong, W. Y.; Chen, P. Roles of Cholesterol in Vesicle Fusion and Motion. *Biophys. J.* **2009**, *97*, 1371–1380.
43. Liu, Y.; Dong, X.; Chen, P. Biological and Chemical Sensors Based on Graphene Materials. *Chem. Soc. Rev.* **2012**, *41*, 2283–2307.
44. Yang, K.; Feng, L.; Shi, X.; Liu, Z. Nano-Graphene in Biomedicine: Theranostic Applications. *Chem. Soc. Rev.* **2013**, *42*, 530–547.
45. Huang, Y.; Chen, P. Nanoelectronic Biosensing of Dynamic Cellular Activities Based on Nanostructured Materials. *Adv. Mater.* **2010**, *22*, 2818–2823.